

Article

Comparison of Dual-Permanent-Magnet-Excited Machines and Surface-Mounted Permanent Magnet Machines in Terms of Force

Minh-Trung Duong ^{1,2}, Do-Hyun Kang ^{2,*}, Yon-Do Chun ^{1,2}, Byung-Chul Woo ², Yoon-Sun Lee ³ and Hwang Wook ²

¹ Energy and Power Conversion Engineering, University of Science and Technology, Daejeon 34113, Korea; Duong.MT@keri.re.kr (M.-T.D.); Ydchun@keri.re.kr (Y.-D.C.)

² Electric Motor Research Center, Korea Electrotechnology Research Institute, Changwon 51543, Korea; Bcwoo@keri.re.kr (B.-C.W.); qwe@keri.re.kr (H.W.)

³ School of Electrical and Electronics Engineering, Chung-Ang University, Seoul 17546, Korea; Dbstudgl@cau.ac.kr

* Correspondence: Dhkang@keri.re.kr; Tel.: +82-055-280-1480

Received: 4 December 2018; Accepted: 8 January 2019; Published: 10 January 2019



Abstract: In this paper, finite element analysis demonstrates the difference between dual-permanent-magnet-excited machines (DPMM) and surface-mounted permanent magnet machines (SPM) in terms of tangential force at the same air gap, diameter, stacking length, and input current. Different from most conventional machines, a novel DPMM has two sets of permanent magnets employed on both stator and rotor. To make a fair comparison, the novel DPMM, based on an original design, is specified to have the same dimensions as a conventional SPM. With the aid of 2D finite element analysis, tangential force generated from the novel DPMM is 167.65% higher than the conventional SPM. To verify the validity of the analyses, a prototype was fabricated and tested. Experiments showed that average deviation was only approximately 1.85%.

Keywords: dual-permanent-magnet-excited machine; surface-mounted permanent magnet machine; force density

1. Introduction

Low-speed permanent magnet (PM) machines have attracted increasing attention in several fields, such as wind power generation, electric vehicles, electric vessels, home appliances, etc. [1–15]. They can offer so-called direct-drive operation, which is beneficial for avoiding disturbances caused by a gearbox [7]. A novel dual-permanent-magnet-excited machines (DPMM) machine, which employs two sets of PMs on both stator and rotor, was proposed and analyzed [3]. Its operating principle lies in bi-directional field modulation, which guarantees effective coupling between the magnetic field excited by the armature windings and those excited by the two sets of PMs. The combination of magnetic gear and conventional PM machines can achieve a high-torque density and also significantly affect torque transmission capability [12]. However, the outer diameter of a conventional DPMM [3] is 269.8 mm, which is larger than a commercial SPM machine in a robotics application. To apply a DPMM model for a low-speed high-torque application, it is necessary to build a compact topology. However, when comparing between different machines, it is difficult to select fair criteria, both in machine configurations and operating conditions. Therefore, this paper focuses on a comparison of a novel DPMM machine and an SPM machine in terms of tangential force density. Various specifications and operating conditions are designed to be the same between these two models to emphasize the advantages of the DPMM machine in terms of tangential force.

Based on the proposed DPMM machine with double excitation from 26 rotor poles and 29 stator poles [3], an equivalent machine is categorized in this paper as having 17 rotor poles and 19 stator poles with the same outward magnetization. The outer diameter was reduced from 269.8 mm to 122 mm after several design steps. A conventional SPM machine with 10 poles and 12 slots was selected as a comparative model. It is well known for its high delivery of precise, cost-effective and maintenance-free motion control, along with high-torque density. Both machines are designed with the same air gap, rotor diameter, stacking length, materials, etc. To have the same current ampere turn (AT), input current on each machine was modified due to the different number of slots.

When both machines are excited at 6120 AT (100%), tangential force density generated by the DPMM machine is significantly higher than that of the SPM machine by approximately 167.65%. All the electromagnetic characteristics are carried out using finite element analyses (FEA) using FLUX-2D software (version 12.3, Altair company, Troy, MI, USA) [16]. To verify the validity of the analyses, an SPM prototype was fabricated and tested. Experimental results show that average deviation was only about 1.85%.

2. Configuration of the Two Comparative Machines

2.1. Dual-Permanent-Magnet-Excited Machine

Figure 1 shows the configuration and dimensions of the equivalent DPMM machine. It should be noted that the winding method is marked as A, B, C for the positive current direction, and A', B', C' for the negative current direction.

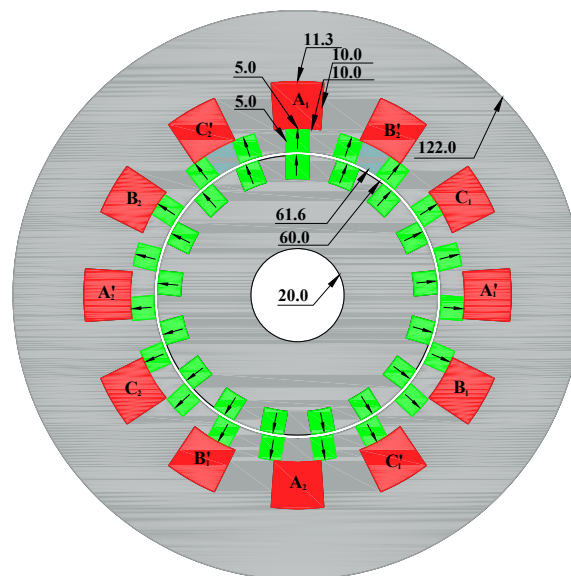


Figure 1. Geometry of the equivalent dual-permanent-magnet-excited machines (DPMM) model (mm).

In its original design, the DPMM consists of 26 rotor PMs, 29 stator PMs, and the winding is distributed according to the phase mark AABBC with 36 slots. The outer diameter of the rotor, the outer diameter of the stator, and the thickness and height of PMs are 178 mm, 269.8 mm, and 10 mm, respectively [3]. These dimensions are significantly larger than a conventional SPM machine used in robot drive applications. For instance, one of the commercial SPM prototype machines currently on the market has a rotor with an outer diameter of 60 mm, a stator with an outer diameter of 95 mm and PMs with a thickness of 4 mm.

The equivalent process of the machine is described by 3 steps:

1. Double PMs: the number of rotor and stator PMs are increased by 2 times to 52 and 58 PMs, respectively. Thickness of PMs is reduced to 5 mm, air gap is 0.8 mm, and phase mark of the winding is modified to ABCABC. The other dimensions are fixed.
2. Haft PMs, slots and dimensions: the number of rotor and stator PMs, rotor and stator diameter, the number of slots is reduced by 2 times. Thickness and height of the PMs are modified to 5 mm.
3. Two third PMs, slots and dimensions: the number of rotor and stator PMs, rotor and stator diameter, the number of slots is reduced by 2/3. These modifications lead to final modified DPMM machine geometry with 17 rotor PMs, 19 stator PMs, 60 mm of outer diameter of rotor, 122 mm of outer diameter of stator, and 12 slots.

The final configuration of the equivalent DPMM machine is presented in Figure 1. Excited PMs are attached on both the stator and rotor part. The rotor PMs are outer-surface inserted into the rotor's iron yoke, while the stator PMs are inner-surface inserted into the stator's iron core. The stator's iron yoke is separated into two parts in order to assemble the excited windings. All parameters of the original and equivalent DPMM models are summarized in Table 1.

Table 1. Dimensions of the studied models.

Configuration	Original DPMM	Equivalent DPMM
Stator PMs, p_1 (pole)	29	19
Rotor PMs, p_2 (pole)	26	17
PMs thickness (mm)	10	5
PMs height (mm)	10	5
Inner diameter of rotor, D_{ri} (mm)	120	20
Outer diameter of rotor, D_{ro} (mm)	178	60
Inner diameter of stator, D_{si} (mm)	179.2	61.6
Outer diameter of stator, D_{so} (mm)	269.8	122
Airgap, g (mm)	0.6	0.8
Number of slots, N_s	36	12
Number of poles, p	6	4
Winding pattern	AABBCC	ABCABC

There are 17 rotor PMs and 19 stator PMs with the same outward-magnetized direction as illustrated in Figure 1. Each PM on the iron forms a pole-pair, hence, the pole-pair number (PPN) or the number of iron teeth on the rotor and stator are $p_1 = 17$ and $p_2 = 19$, respectively. The armature windings are configured in 12 coils, and each coil is assumed to be wound by one turn and excited by a current value equal to 6120 AT, which produces $p_3 = 2$ pole pairs. Accordingly, the magnetic field excited by the PMs on the rotor is expressed as:

$$PPN_{(i,j)}^r = |(2i - 1)p_1 + jp_2| \quad (1)$$

where $i = 1, 2, 3 \dots, \infty$ and $j = \pm 1, \pm 2, \pm 3, \dots, \pm \infty$.

The rotational speed of the harmonic component can be given by:

$$\omega_{(i,j)}^r = \frac{(2i - 1)p_1}{(2i - 1)p_1 + jp_2} \Omega_r \quad (2)$$

where Ω_r is rotational speed of the rotor.

Similarly, the magnetic field excited by the stator and the rotational speed of harmonics is expressed as:

$$PPN_{(i,j)}^s = |(2i - 1)p_2 + jp_1| \quad (3)$$

$$\omega_{(i,j)}^s = \frac{jp_1}{(2i - 1)p_2 + jp_1} \Omega_r \quad (4)$$

Finally, the magnetic field excited by armature windings on the stator are considered:

$$PPN_{(i,j)}^{w,r} = |(2i - 1)p_3 + jp_1| \quad (5)$$

$$\omega_{(i,j)}^{w,r} = \frac{(2i - 1)p_3}{(2i - 1)p_3 + jp_1} \Omega_r + \frac{jp_1}{(2i - 1)p_3 + jp_1} \Omega_r \quad (6)$$

It should be noted that the relation between the PPN of the stator, rotor and winding is satisfied with (7):

$$p_2 = p_1 + p_3 \quad (7)$$

Based on the proposed structure, if the machine is excited by only rotor PMs, stator PMs, or stator winding, the order of the fundamental magnetic field is 17, 19 or 2, respectively. The verification of the fundamental magnetic field was verified by simulation in Reference [3].

2.2. Surface-Mounted Permanent Magnet Machine

Figure 2 schematically presents the configuration of a 10-pole, 12-slot SPM machine.

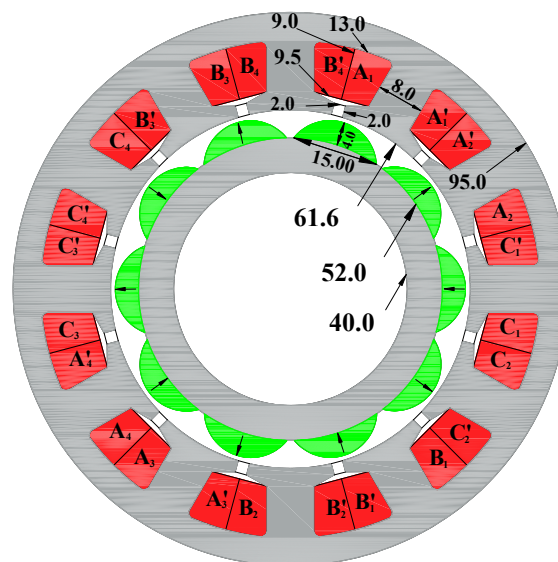


Figure 2. Geometry of the surface-mounted permanent magnet machines SPM model (mm).

The major advantages of the SPM machine are high torque with a compact design, high power through maximum copper fill factor, low loss through optimized stator and rotor design, highly precise controllability, etc. Therefore, the SPM machine is used for many industrial applications and mechatronic drives. The machine in Figure 2 is composed of the circle-shape magnets, three phases of armature winding, and double layers of slots. In order to have a fair comparison, the SPM machine is assumed to be wound by 1 turn on each slot with an excited current of 6120 AT.

3. Optimal Design of the DPMM Machine

3.1. Original Design of The DPMM

For a fair comparison, all machine concepts are modeled with the same conditions. The major similarities are given in Table 2.

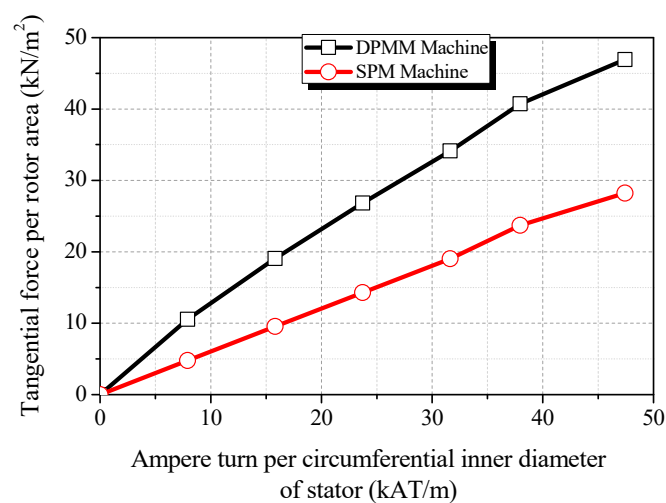
Table 2. Description of the two models for comparison.

Items	DPMM	SPM
Stacking length, L_{st} (mm)		90
Outer diameter of rotor, D_{ro} (mm)		60
Outer diameter of stator, D_{so} (mm)	122	95
Air gap, g (mm)		0.8
Electrical steel sheet		35PN380
Permanent magnet material	NdFeB – $B_r = 1.2T$; $\mu_r = 1.05$ at 20 °C	
Copper fill factor, k_{fill}		50%
Total current ampere-turn (100%)		6120AT
(rms current per slot * number of slot)		(510 × 12)

The stacking length of both of the comparative machines is 90 mm, and the outer diameter of the rotor is 60 mm. The iron core is made of magnetic steel 35PN380 provided by POSCO company. The rated rotating speed is 1800 rpm, and the total input current ampere turn is 6120 AT. To simplify the simulation, it is assumed that there is only one wire per slot and the fill factor is 50%. Therefore, RMS input current to the DPMM and SPM machine is 510 A and 255 A, respectively.

Figure 3 and Table 3 show the differences between the two comparative machines for different input current in terms of torque T and tangential force density F_{td} . When the input current is 6120 AT (100%), the ampere-turn per circumferential inner diameter of stator can be calculated as follows:

$$AT_{STT} = \frac{6120}{2\pi \times 30.8 \times 10^{-3}} = 31.6(\text{kAT/m}) \quad (8)$$

**Figure 3.** Tangential force density comparison for different input currents.**Table 3.** Tangential force density comparison.

Current (AT)	Output Torque (Nm)		Tangential Force Per Rotor Area (kN/m ²)	
	DPMM	SPM	DPMM	SPM
0 (0%)	0.00	0.00	0.00	0.00
1530 (25%)	5.37	2.43	10.55	4.77
3060 (50%)	9.70	4.86	19.06	9.55
4590 (75%)	13.66	7.28	26.84	14.30
6120 (100%)	17.36	9.69	34.11	19.04
7650 (125%)	20.72	12.06	40.71	23.70
9180 (150%)	23.87	14.36	46.90	28.22

The tangential force F_t is obtained from FEA software. If one refers the tangential force F_t to the active surface in order to obtain some feeling for the magnitude of the tangential force density F_{td} , magnitude of the tangential force density F_{td} can be derived by [6,11]:

$$F_{td} = \frac{\text{Tangential force}}{\text{Rotor surface area}} = \left(\frac{T}{r}\right) / (2\pi r L_{st}) = \frac{T}{2\pi r^2 L_{st}} \quad (9)$$

where r (30 mm) is outer radius of the rotor and T is torque.

For instance, when the input current ampere turn is 6120 AT (100%), tangential force density can be calculated as:

$$F_{td} = \frac{17.36 \times 10^{-3}}{2\pi \times 0.03^2 \times 0.09} \approx 34.1 \text{ (kN/m}^2\text{)} \quad (10)$$

Under 100% input current, the DPMM provides a tangential force per rotor area of 34.1 kN/m², while the SPM machine can generate only 19.0 kN/m². The output torque and tangential force density increase linearly with the input current.

It can be clearly seen from Figure 4 that the tangential force density F_{td} of the DPMM increases dramatically when the air gap length is decreased from 1.0 mm to 0.3 mm. When the air gap $g = 0.3$ mm, the tangential force density produced by the DPMM machine is higher by 159.3% in comparison with the SPM machine. These results suggest that the DPMM can be considered as a prospective candidate as a low-speed high-torque machine.

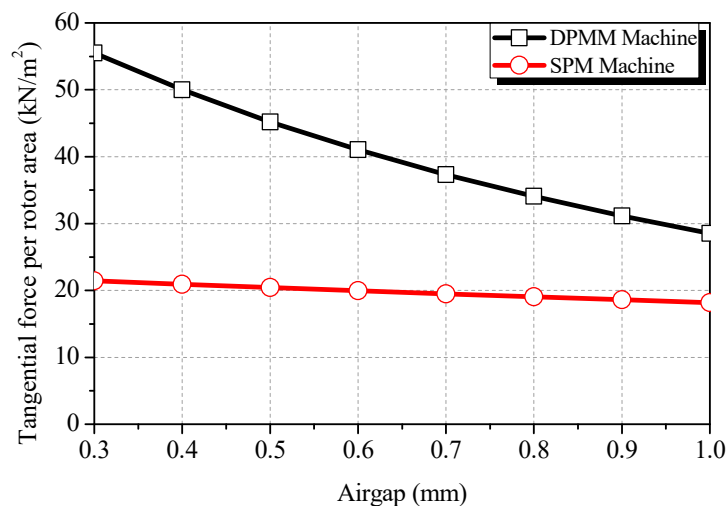


Figure 4. Tangential force density comparison for different air gap lengths.

It is a controversy that the increase in the force density produced by the DPMM machine comes from a higher volume of the PMs, which is the most expensive material when fabricating a machine. However, the effectiveness should be compared in terms of the tangential force per volume of the PMs. The total volume of the PMs for the SPM and DPMM machine is estimated at $547.2 \times 10^{-6} \text{ m}^3$ and $742.2 \times 10^{-6} \text{ m}^3$, respectively. Under rated conditions, tangential force density based on the volume of PMs from DPMM and SPM machines is 24.0 kN/m^3 and 17.7 kN/m^3 , respectively. This means that with the same volume of the PM, tangential force density generated from the DPMM is higher than that of a conventional SPM by approximately 26.3%.

3.2. Optimal Design of the DPMM

In an optimal design, the dimensions of the DPMM are studied in order to reduce the magnet volume and iron core, which reduces the cost, but the tangential force density is still controlled at an acceptable value with a deviation of around 5%. As shown in Figure 5, there are three main dimensions

to be considered: distance between coil and outer diameter of stator a (or including outer diameter of stator), height of PM b , and height of slot c .

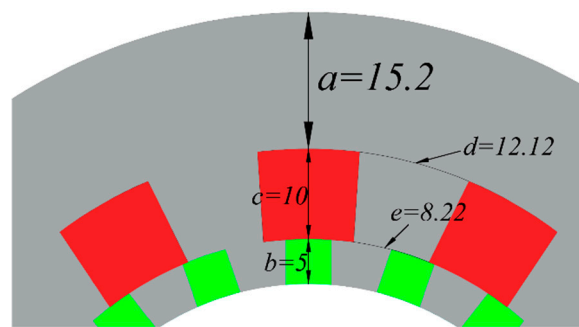


Figure 5. Original dimensions.

Firstly, the outer diameter of the original stator is reduced to be the same as that of the SPM machine (95 mm). The modification is described in Figure 6 by variation of the distance a between the outer slot perimeter and the outer diameter of the stator. This value is decreased from 15.2 mm to 1.7 mm, which means the outer diameter of the stator is decreased from 122 mm to 95 mm. In Figure 6, at the selected point $a = 4.2$ mm, tangential force density decreases dramatically by 6.7% from 33.07 kN/m^2 to 30.87 kN/m^2 (thus, the outer diameter of the stator is 100 mm). This can be named as a knee-point.

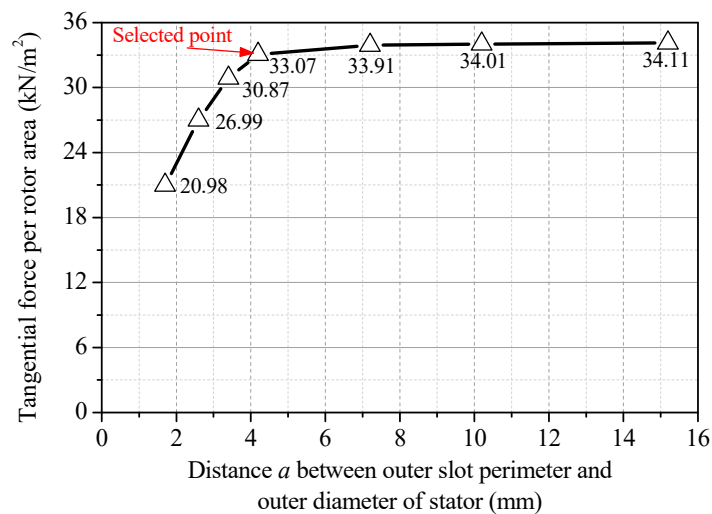


Figure 6. Tangential force density versus the distance a between the outer slot perimeter and the outer diameter of the stator.

The second modified dimension is the height b of the stator magnets, which is 5 mm. Figure 7 illustrates the variation of tangential force density (when $a = 4.2$ mm). At the selected point $b = 4$ mm, tangential force density is decreased by approximately 5.5%.

Slot shape is the last modification point where the target is similar to the value of e and d as illustrated in Figure 5. In addition, the circle corner shape is preferred in conventional machines instead of the original square corner shape. However, the slot area is fixed in all modifications. By fixing the previous selection, slot shape and also slot height c is to be considered. According to Figure 8, when the slot shape is modified to circle corner shape, the tangential force density increases by 2.9%. In general, tangential force density decreases slightly when slot height varies from 10 mm to 8 mm. At the selected point, the distance between the slot of the inner perimeter and outer perimeter is $e = 8.22$ mm and $d = 9.22$ mm, respectively. This dimension can be accepted, according to the original design target.

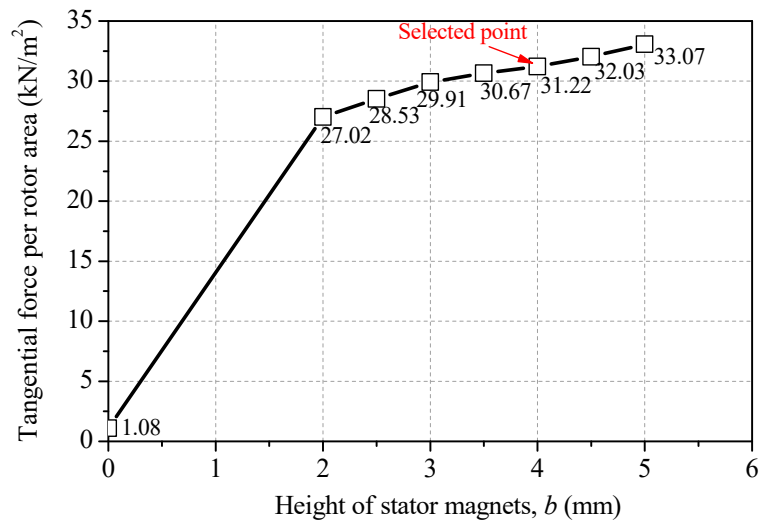


Figure 7. Tangential force density versus the height b of the stator magnets.

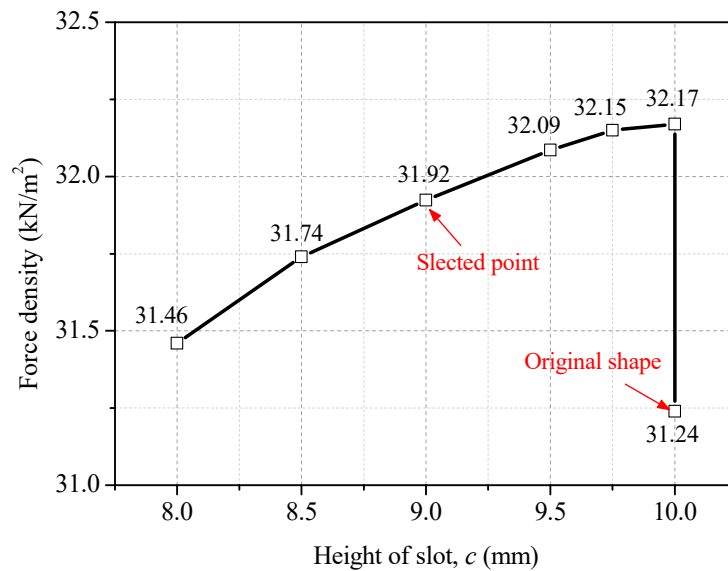


Figure 8. Tangential force density versus the slot height c .

In the FEM analysis, the final design of the DPMM was modeled as presented in Figure 9. To increase the accuracy of the calculation, four air gap layers were created and the second order mesh was applied. Overall, the number of mesh elements is 40,100 and the number of excellent quality elements is about 99.56%. Flux distribution on the DPMM is shown in Figure 10.

Characteristics of the two compared models are presented in Table 4. According to the optimal design, the tangential force density generated by the DPMM machine has an advantage of 167.65% over the SPM machine. In addition, torque per motor volume from the DPMM machine is also significantly higher by 51.3% than that from the SPM machine. However, major drawbacks of the DPMM machine lie in the higher iron losses (101.91 W) and lower power factor (0.62).

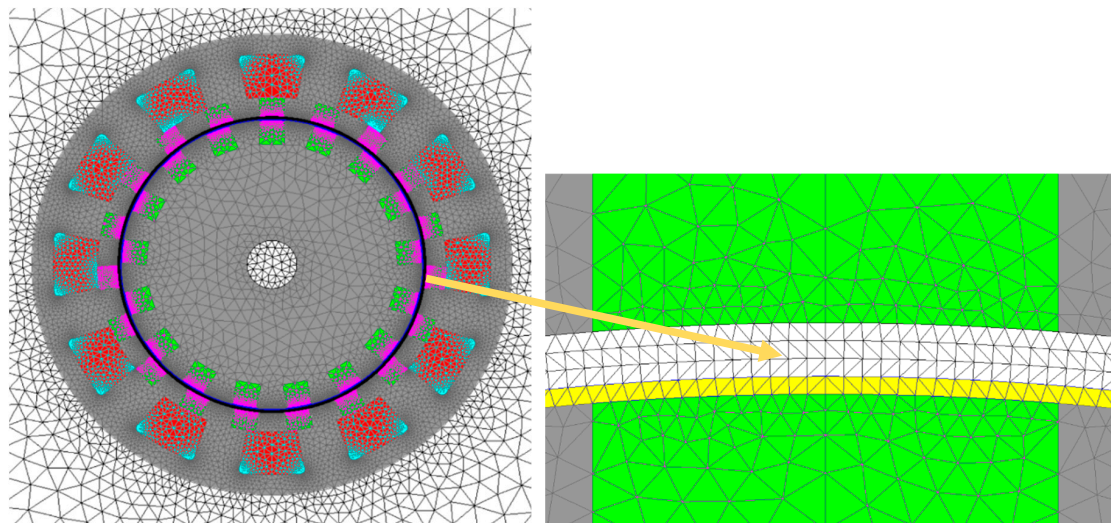


Figure 9. Final DPMM design with mesh distribution.

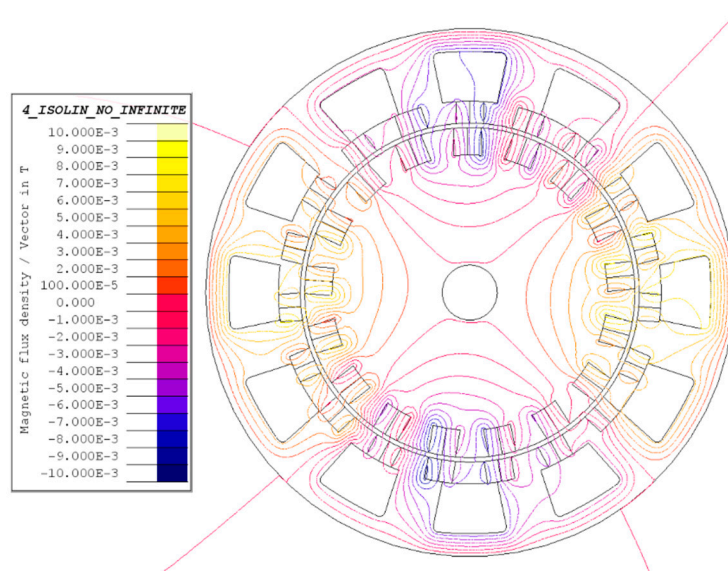


Figure 10. Flux distribution on the DPMM.

Table 4. Characteristics of the two studied models.

Parameters	Optimal DPMM	SPM
Inner diameter of rotor, D_{ri} (mm)	20	40
Outer diameter of rotor, D_{ro} (mm)		60
Inner diameter of stator, D_{si} (mm)		61.6
Outer diameter of stator, D_{so} (mm)	100	95
Air gap, g (mm)		0.8
Total current ampere-turn (100%)		6120
Copper fill factor, k_{fill} (%)		50
Number of slot, N_s		12
Electrical steel sheet		35PN380
Permanent magnet		NdFeB – $B_r = 1.2T$; $\mu_r = 1.05$ at 20 °C
Tangential force density, (kN/m ²) (at 100% current ampere turn)	31.92	19.04
Torque/volume, (kN/m ³) (rotor torque per motor total volume)	45.16	29.85
Iron losses (W)	101.91	15.84
Power factor	0.62	0.95

4. Validation by Experiment

Because of its complexity, the DPMM machine has not been successfully fabricated. However, there is an acceptable solution to validate the accuracy and reliability of the simulation mentioned in Reference [17]. In Reference [17], there were four comparative models, but it was impossible to fabricate the proposed machines, although they would be able to offer good performance. Therefore, a different phase full TFM model was built and validated with FEM analyses.

Similarly, based on an existing SPM machine in the laboratory with a similar configuration to the comparative SPM machine in this paper, validation of the analyses was performed. The geometry of both SPM models is compared in Table 5.

Table 5. Characteristics of the two studied models.

Items	Compared SPM	Commercial SPM
Staking length, L_{st} (mm)	90	31
Outer diameter of rotor, D_{ri} (mm)	60	63.5
Inner diameter of stator, D_{si} (mm)	61.6	66
Outer diameter of stator, D_{so} (mm)	95	100
Air gap, g (mm)	0.8	1.25
Number of turns/slot	1	15

Figure 11 shows the prototype and Figure 12 shows the experimental setup. When rotating speed varies from 0 to 2750 rpm, no-load induced voltage back EMF is linearly increased as shown in Figure 13. The average deviation was estimated to be about 1.85%. A similar tendency can be seen in Figure 14; when the input current ampere turn is increased from 0% to 140%, average deviation of the output torque is approximately 1.42%. This very low deviation suggests that the analysis data is reliable and acceptable.

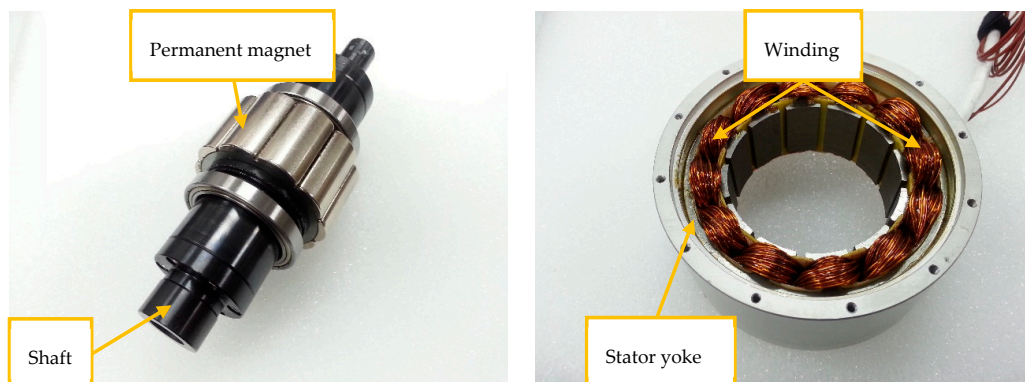


Figure 11. Prototype.

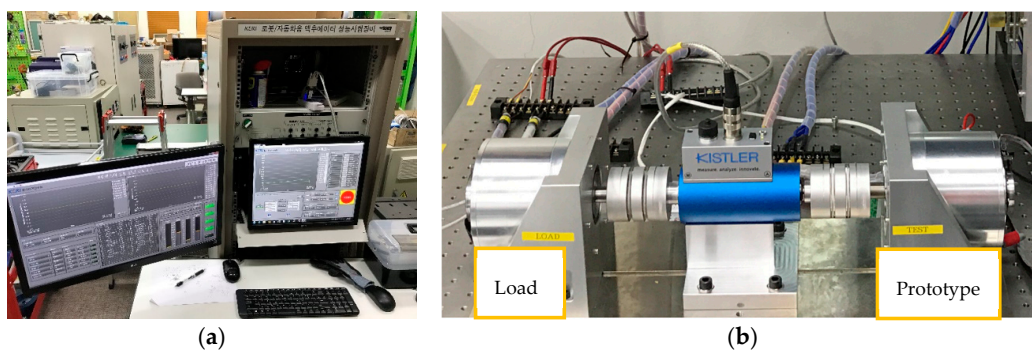


Figure 12. Experimental setup: (a) Human machine interface; (b) back-to-back system.

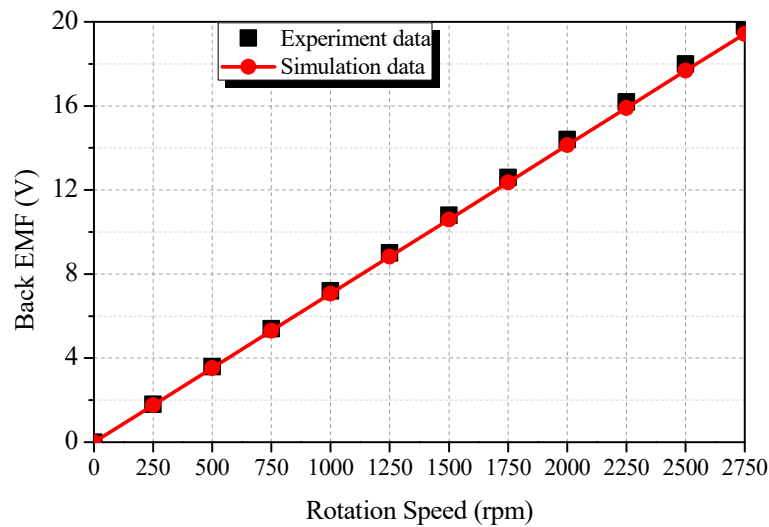


Figure 13. Back EMF for different rotating speeds.

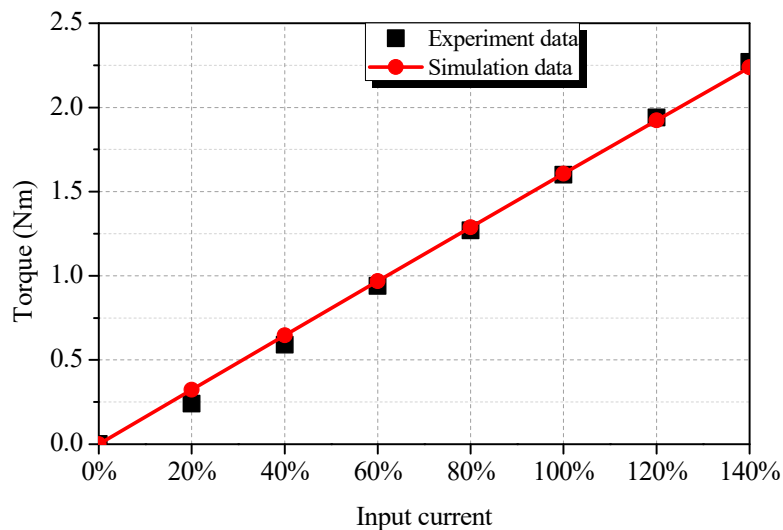


Figure 14. Torque for different input currents.

5. Conclusions

The tangential force between the dual-permanent magnet excited machine (DPMM) and the surface-mounted permanent magnet (SPM) was compared under fair conditions. In order to better understand the magnitude of the tangential force per unit area, the tangential force density was derived by equation and calculated by the ampere-turn per circumferential inner diameter of the stator.

Under 100% of the input current ampere turn (6120 AT), the optimized DPMM machine achieves 167.65% higher tangential force density than the conventional SPM machine. This difference can be increased dramatically when the air gap length is decreased or the input current is increased. For example, in the original design of the DPMM machine, when the air gap length is 0.3 mm, the tangential force density is higher than the conventional SPM machine by 159.3%. When considering tangential force per permanent magnet volume, the DPMM can possibly generate a higher force density value by nearly 35.6%. In low-speed high-torque or robot drive applications, the DPMM is a promising candidate.

Although the DPMM prototype has not been successfully fabricated, the reliability of the analysis data was experimentally proved using the proposed approach in the other paper. The results of the experiment confirmed an excellent agreement with very low deviation for back EMF and torque.

The main disadvantage of the novel DPMM machine is high core loss according to the higher input current frequency. This also leads to an increase in cost given the high volume of magnets and high quality core-steel, for example, cobalt steel [18].

In practice, some other aspects such as iron loss, power factor, thermal analysis, etc., which are not studied in detail in this comparison, will be considered for an optimal design using both 2D and 3D finite element methods.

Author Contributions: Conceptualization, D.-H.K.; software, M.-T.D., validation; M.-T.D., writing, M.-T.D.; supervision, Y.-D.C.; administration, B.-C.W.; investigation, Y.-S.L.; data curation, H.-W.

Funding: This work was supported by the KERI's Primary Research Program of MSIP/NST (No. 18-12-N0101-25).

Conflicts of Interest: The authors declare no conflicts of interest.

References

- Ahmad, M.; Khan, M.R.; Iqbal, A. A Doubly Fed Induction Motor as High Torque Low Speed Drive. In Proceedings of the 2006 International Conference on Power Electronic, Drives and Energy Systems, New Delhi, India, 12–15 December 2006; pp. 1–3.
- Kawamura, W.; Chen, K.; Hagiwara, M.; Akagi, H. A Low-Speed, High-Torque Motor Drive Using a Modular Multilevel Cascade Converter Based on Triple-Star Bridge Cells (MMCC-TSBC). *IEEE Trans. Ind. Appl.* **2015**, *51*, 3965–3974. [CrossRef]
- Jian, L.; Shi, Y.; Liu, C.; Xu, G.; Gong, Y.; Chan, C.C. A Novel Dual-Permanent-Magnet-Excited Machine for Low-Speed Large-Torque Applications. *IEEE Trans. Magn.* **2013**, *49*, 2381–2384. [CrossRef]
- Liu, X.; Zhong, X.; Du, Y.; Chen, X. A Novel Triple-Permanent-Magnet-Excited Vernier Machine with Double-Stator Structure for Low-Speed and High-Torque Applications. *Energies* **2018**, *11*, 1713. [CrossRef]
- Zou, T.; Li, D.; Qu, R.; Jiang, D.; Li, J. Advanced High Torque Density PM Vernier Machine With Multiple Working Harmonics. *IEEE Trans. Ind. Appl.* **2017**, *53*, 5295–5304. [CrossRef]
- Kang, D.H.; Chun, Y.H.; Weh, H. Analysis and optimal design of transverse flux linear motor with PM excitation for railway traction. *IEE Proc. Electr. Power Appl.* **2003**, *150*, 493–499. [CrossRef]
- Jian, L.; Xu, G.; Mi, C.C.; Chau, K.T.; Chan, C.C. Analytical Method for Magnetic Field Calculation in a Low-Speed Permanent-Magnet Harmonic Machine. *IEEE Trans. Energy Convers.* **2011**, *26*, 862–870. [CrossRef]
- Sato, K.; Shin, J.; Koseki, T.; Aoyama, Y. Basic experiments for high-torque, low-speed permanent magnet synchronous motor and a technique for reducing cogging torque. In Proceedings of the XIX International Conference on Electrical Machines—ICEM 2010, Rome, Italy, 6–8 September 2010; pp. 1–6.
- Mese, E.; Yasa, Y.; Ertugrul, B.T.; Sincar, E. Design of a high performance servo motor for low speed high torque application. In Proceedings of the 2014 International Conference on Electrical Machines (ICEM), Berlin, Germany, 2–5 September 2014; pp. 2014–2020.
- Vukotić, M.; Miljavec, D. Design of a permanent-magnet flux-modulated machine with a high torque density and high power factor. *IET Electr. Power Appl.* **2016**, *10*, 36–44. [CrossRef]
- Kang, D.H.; Weh, H. Design of an integrated propulsion, guidance, and levitation system by magnetically excited transverse flux linear motor (TFM-LM). *IEEE Trans. Energy Convers.* **2004**, *19*, 477–484. [CrossRef]
- Atallah, K.; Calverley, S.D.; Howe, D. Design, analysis and realisation of a high-performance magnetic gear. *IEE Proc. Electr. Power Appl.* **2004**, *151*, 135–143. [CrossRef]
- Ji, J.; Zhao, J.; Zhao, W.; Fang, Z.; Liu, G.; Du, Y. New High Force Density Tubular Permanent-Magnet Motor. *IEEE Trans. Appl. Supercond.* **2014**, *24*, 1–5. [CrossRef]
- Artetxe, G.; Paredes, J.; Prieto, B.; Martinez-Iturralde, M.; Elosegui, I. Optimal Pole Number and Winding Designs for Low Speed–High Torque Synchronous Reluctance Machines. *Energies* **2018**, *11*, 128. [CrossRef]
- Xiao-hai, L.; Zhu, L.; Ji-min, Z.; Jiang, S. Research on special low-speed, high-torque permanent magnet synchronous motor for screw pump. In Proceedings of the 2009 IEEE 6th International Power Electronics and Motion Control Conference, Wuhan, China, 17–20 May 2009; pp. 1858–1862.
- Flux 2D/3D Fast and Robust Electromagnetic, Electric and Thermal Solver. Available online: <https://altairhyperworks.com/product/flux/Capabilities---Robust-Solver> (accessed on 4 December 2018).

17. Hoang, T.; Kang, D.; Lee, J. Comparisons Between Various Designs of Transverse Flux Linear Motor in Terms of Thrust Force and Normal Force. *IEEE Trans. Magn.* **2010**, *46*, 3795–3801. [[CrossRef](#)]
18. Seite Nicht Gefunden—VACUUMSCHMELZE GmbH & Co. KG. Available online: <https://www.vacuumschmelze.de/404.html> (accessed on 4 December 2018).



© 2019 by the authors. Licensee MDPI, Basel, Switzerland. This article is an open access article distributed under the terms and conditions of the Creative Commons Attribution (CC BY) license (<http://creativecommons.org/licenses/by/4.0/>).